# AIAA 2001–0425
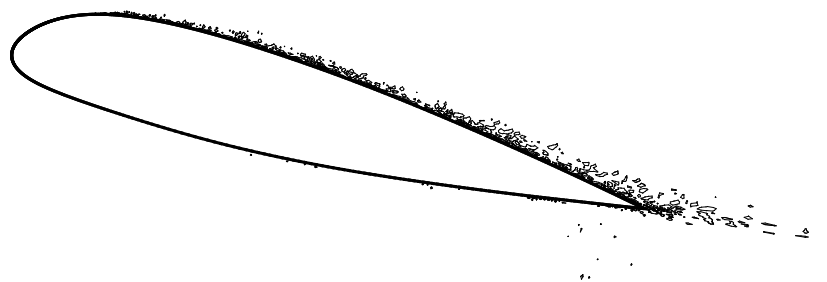
# LARGE EDDY SIMULATION OF THE FLOW AROUND AN AIRFOIL

S. Dahlström and L. Davidson
Department of Thermo and Fluid Dynamics
Chalmers University of Technology
SE-412 96 Göteborg, Sweden

# 39th AIAA Aerospace Sciences Meeting and Exhibit
## 8–11 January 2001 / Reno, NV

# LARGE EDDY SIMULATION OF THE FLOW AROUND AN AIRFOIL

S. Dahlström and L. Davidson
Department of Thermo and Fluid Dynamics
Chalmers University of Technology
SE-412 96 Göteborg, Sweden

**The work presented in this paper is part of the ongoing Brite-Euram project LESFOIL. The feasibility of Large Eddy Simulation (LES) of flows around simple, two-dimensional airfoils is investigated in the project. The specific case chosen is the subsonic flow ($Ma_\infty = 0.15$) around the Aerospatiale A-profile at an incidence of $13.3°$ and at a chord Reynolds number of $2.1 \cdot 10^6$. The method used is an incompressible implicit second-order finite volume method with a collocated grid arrangement. Computations have been carried out on a mesh consisting of $721 \times 65 \times 33$ nodes in the streamwise, wall-normal and spanwise direction, respectively. As subgrid scale (SGS) models the one-equation SGS model by Yoshizawa and the Smagorinsky model are used. To suppress unphysical oscillations, a bounded second-order upwind scheme is used in front of the airfoil and upstream of the transition point. In the transition region, it is gradually mixed with the central difference scheme (CDS). The non-dissipative CDS gives rise to numerical oscillations and the boundary layer is tripped numerically. The treatment of the SGS models in the transition region is highlighted in the paper. With the present treatment of the transition, it either takes place too far downstream or it is too anisotropic and unphysical.**

## Introduction

The feasibility of Large Eddy Simulations (LES) of flows around simple, 2D airfoils is investigated in the LESFOIL project (see Ref. 1, where the project is presented). The airfoil case chosen is the flow around the Aerospatiale A-airfoil at an angle of attack, $\alpha$, of 13.3°. The chord Reynolds number is $2.1 \cdot 10^6$ and the flow is subsonic with a freestream Mach number of $0.15$. These are high-lift conditions at take-off and landing. The flow around the Aerospatiale A-airfoil has been the subject of extensive study. Different CFD codes (steady and unsteady RANS, compressible and incompressible methods) were validated in the EUROVAL project[2] and in the ECARP project[3] on this particular single-element airfoil. It was found that few RANS models are capable of handling this flow problem, mainly because of the lack of curvature effects in the eddy-viscosity models. The second-moment closures (which do take into account curvature effects) produced the best results, see also Refs. 4–6. Much because of the rate at which computer power is increasing, LES is becoming an interesting approach applicable for more complex flows.

This is a challenging case for LES owing to the high Reynolds number and because of the different flow regimes around the airfoil, which are sketched in Fig. 1. At the leading edge there is a very thin laminar boundary layer. On the

pressure side, this boundary layer is tripped at 30 % of the chord and there is a transition to a very thin turbulent boundary layer. On the suction side, there is a peak in the pressure near the leading edge. The favorable pressure gradient accelerates the flow around the leading edge. In this case the flow separates, a separation bubble is formed and, when the flow reattaches at about 12 % of the chord, the boundary layer becomes turbulent. The boundary layer grows under the influence of an adverse pressure gradient and, at about 82.5 % of the chord, the flow separates. In the wake, downstream of the trailing edge, the low-speed flow from the separation region on the suction side forms a mixed shear layer with the flow from the very thin boundary layer on the pressure side.

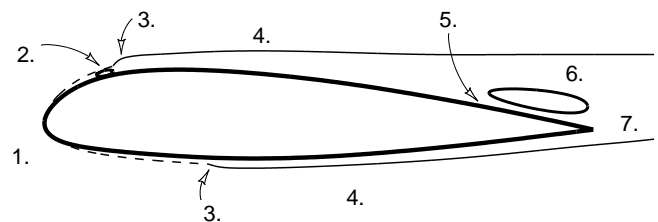In an LES, you wish to resolve all the *impor-*



**Fig. 1    Schematic sketch of the flow regimes around the Aerospatiale A-profile: 1. laminar boundary layer, 2. laminar separation bubble, 3. transition region, 4. turbulent boundary layer, 5. separation point, 6. separation region, 7. wake region.**

*tant* flow structures and the small-scale turbulence is modeled. Ideally, you would like to resolve all the different flow regimes plotted in Fig. 1: the laminar boundary layer with a sufficient amount of nodes (in the streamwise and wall-normal direction), the recirculation regions (the transitional and the one at the trailing edge) and also the turbulent boundary layer. Important flow structures in the turbulent boundary layer include the near-wall streaks in the viscous sublayer and energy-producing structures in the buffer region. In a *wall-resolved* LES, these coherent structures can be captured if the sizes of the cells closest to the wall are within the range of $50 < \Delta x^+ < 150$ and $15 < \Delta z^+ < 40$ (expressed in wall units $(\frac{u_\tau}{\nu})$ in the streamwise and spanwise direction, respectively) and if the near-wall node, $y^+$, is located at a wall distance of $y^+ < 2$.[7] A wall-resolved LES of the near-wall streaks in the turbulent boundary layer is not feasible because of the required computer power. At this high Reynolds number, the *near-wall problem* of LES is evident and the use of approximate wall boundary conditions is needed. If wall functions are used, in which the effect of the energy-producing structures near the wall are modeled (rather than resolved), grids with a coarser resolution can be used. However, the resolution still needs to be fine enough to capture the *important* large-scale turbulence. That is, the resolved turbulence should at least reach the inertial subrange (to be able to model the fine-scale turbulence with SGS models). Perhaps it is fair to assume that it is equally important with the resolution of the boundary layer at e.g. 70 % of the chord as it is at e.g. 20 %. This reasoning leads to a requirement on the number of nodes per boundary layer thickness. By using Spalarts 20-nodes per boundary-layer thickness estimate in each direction,[8] $50 - 100$ million nodes are needed.[9] The very thin boundary layer, just downstream of the transitional separation bubble, is the cause for this high amount of required nodes.

In the present computations a very coarse mesh is used, e.g. the laminar separation bubble is barely resolved. Yet, the wall-normal cell size, $\Delta y$, is too small to allow wall functions in which the first node is located in the logarithmic region of the turbulent boundary layer (it is small enough to be able to capture the trailing edge separation bubble). The near-wall node is located in the buffer region ($5 \leq y^+ \leq 30$) and wall functions are needed that are applicable in this region. With this resolution, is it possible to prescribe the transition and the development of the turbulent boundary layer just downstream of the transition region? Two SGS models are used in the computations presented in this paper. The behaviour of the models, especially in the transition region is highlighted. The next section summarizes the numerical method. The upwinding/central difference scheme and the SGS models used are presented. The mesh, parallelization and boundary conditions are described in the section *Computational Setup*. Finally the results are presented and in the last section conclusions are drawn.

## Numerical Method

The code used is an incompressible finite volume Navier-Stokes solver called CALC-BFC.[10] The solver is based on structured grids and the use of curvi-linear boundary fitted coordinates. The grid arrangement is collocated and the Rhie and Chow interpolation method[11] is used. The code is parallelized for 3D flows[12] using block decomposition and the message passing systems PVM and MPI. The PISO algorithm[13] is used for the pressure-velocity coupling, with two additional corrector steps beside the first SIMPLE step.

In LES, the large eddies are solved and the small scales are modeled. Filtering of the incompressible continuity and momentum equations results in

$$\frac{\partial \overline{u}_i}{\partial x_i} = 0 \quad (1)$$

$$\frac{\partial \overline{u}_i}{\partial t} + \frac{\partial}{\partial x_j}(\overline{u}_i \overline{u}_j) = -\frac{1}{\rho}\frac{\partial \overline{p}}{\partial x_i} + \frac{\partial}{\partial x_j}\left[\nu \frac{\partial \overline{u}_i}{\partial x_j} - \tau_{ij}\right] \quad (2)$$

$$\tau_{ij} = \overline{u_i u_j} - \overline{u}_i \overline{u}_j \quad (3)$$

Here, $\tau_{ij}$ are the subgrid scale (SGS) stresses. They are the contribution of the small scales, the unresolved stresses, and are unknown and must be modeled.

### Smagorinsky SGS Model

One of the SGS models used in the computations is the Smagorinsky model.[14] The subgrid scales are of the order of the filter width, $\Delta$, and, by using the eddy viscosity assumption and mixing length theory, the anisotropic part of $\tau_{ij}$ is modeled, according to Smagorinsky, as:

$$\tau_{ij} - \frac{1}{3}\delta_{ij}\tau_{kk} = -2\nu_{sgs}\overline{S}_{ij} \quad (4)$$

$$\nu_{sgs} = (C_S \Delta)^2 |\overline{S}| \quad (5)$$

$$|\overline{S}| = \sqrt{2\overline{S}_{ij}\overline{S}_{ij}} \quad (6)$$

Here, $\overline{S}_{ij} = \frac{1}{2}\left(\frac{\partial \overline{u}_i}{\partial x_j} + \frac{\partial \overline{u}_j}{\partial x_i}\right)$ is the filtered strain rate and $\nu_{sgs}$ is the Smagorinsky eddy viscosity. The Smagorinsky constant, $C_S$, is equal to $0.1$ in the computations. The filter width, $\Delta$, is computed using the definition $\Delta^3 = \Delta x \Delta y \Delta z = \delta V$, i.e. $\Delta$ is taken as the cubic root of the volume of a finite volume cell.

### Yoshizawas One-Equation SGS Model

The second SGS model used in the computations is the one-equation SGS model by Yoshizawa,[15] which reads:

$$\frac{\partial k_{sgs}}{\partial t} + \frac{\partial}{\partial x_j}(\bar{u}_j k_{sgs}) = \qquad (7)$$

$$\frac{\partial}{\partial x_j}\left[(\nu + \nu_{sgs})\frac{\partial k_{sgs}}{\partial x_j}\right] + P_{k_{sgs}} - C_\varepsilon \frac{k_{sgs}^{3/2}}{\Delta}$$

$$P_{k_{sgs}} = 2\nu_{sgs}\bar{S}_{ij}\bar{S}_{ij}, \; \nu_{sgs} = C_k \Delta k_{sgs}^{1/2} \qquad (8)$$

Here, the filter width, $\Delta$, is taken as the minimum size of the cell, i.e. $\Delta = \min\{\Delta x, \Delta y, \Delta z\}$. The constants are $C_k = 0.07$ and $C_\varepsilon = 1.05$.

### Treatment of the Transition

The filtered momentum equations (Eqs. 2) are discretized in time using the Crank-Nicolson scheme and in space using 2nd order difference schemes (the central difference scheme (CDS) and the van Leer scheme).

When the momentum equations are discretized in space using the central difference scheme (CDS), considerable unphysical oscillations are present all over the computational domain. The CDS is often used in LES because of its non-dissipative and energy-conserving properties. However, the scheme is also known to produce these odd-even oscillations (grid-to-grid oscillations or wiggles) when the resolution is poor.

To remove the unphysical oscillations in front of the airfoil and upstream of the transition region, a bounded second-order upwind discretization scheme (the van Leer scheme) is used in this region. The schemes are blended in the transition region, so that the convective flux can be expressed as:

$$\dot{m}u_{UDS}^m + \dot{m}\left[\alpha u_{CDS}^{m-1} - \alpha u_{UDS}^{m-1} + (1-\alpha)u_{UDScorr}^{m-1}\right] \quad (9)$$

Here, $CDS$ stands for the central difference scheme, $UDS$ for the 1st-order upwind scheme and $UDScorr$ for the 2nd-order correction to the lower order upwind scheme ($m-1$ is the previous iteration). Here $\alpha$ is a blending function ($0 \le \alpha \le 1$) and, at the extremes, we have:

$\alpha = 0$:  the van Leer scheme
$\alpha = 1$:  the central difference scheme
          with deferred correction

The blending function used in the computations blends the two schemes from 2 to 12 % of the chord on the suction side and from 17 to 30 % on the pressure side. Upwinding removes unphysical oscillations, not only in the part of the domain where upwinding is used but also downstream of the area where the mixing between the two schemes is applied.[16, 17]

Not only the discretization of the convective terms has an effect on the transition but also the treatment of the SGS models. For example the eddy viscosity from the Smagorinsky model does not disappear in laminar flows (unless the strain tensor is zero). This results in additional dissipation in the laminar region (besides the one from the upwinding scheme). Here, in the Smagorinsky model, the Smagorinsky eddy viscosity is set to zero upstream of 2 % of the chord on the suction side and is gradually mixed with the eddy viscosity downstream of that point. At the location of the transition given in the experiments (at 12 % of the airfoil chord) the Smagorinsky model is fully active. In the one-equation SGS model the SGS kinetic energy, $k_{sgs}$, is set to zero upstream of the transition point and there is no damping or blending in the $k_{sgs}$-equation. However, the eddy viscosity from the one-equation model is not fully active until 23 % of the chord. Similar approaches are applied around the transition point on the pressure side of the airfoil.

## Computational Setup

### The Mesh

The computations have been conducted on a mesh consisting of $721 \times 65 \times 33$ nodes in the streamwise, wall-normal and spanwise direction, respectively. In the streamwise direction, 302 nodes are placed along the suction side of the airfoil and 200 nodes along the pressure side. Fig. 2 shows zooms of the C-mesh. The outer boundaries are located approximately ten chord lengths away from the airfoil.

The height of the cell at the leading edge is $0.00026c$ and this height is kept approximately constant along the suction side of the profile. The length of the cells at the leading edge is $0.0010c$ and $0.0050c$ at the trailing edge. The streamwise grid spacing, $\Delta x$, is increased linearly from the leading to the trailing edge. The stretching is very low (which is crucial for the energy conservation[18]). Overall, the stretching in this direction is less than 5.9 % (the maximum is in the wake near the trailing edge). Also, the mesh is refined along the wake.

The extent in the spanwise direction is chosen as $L_z = 0.12c$. When periodic boundary conditions are used, these conditions imply that the extent in the spanwise direction should be wider than the largest structures in that direction. The largest scales in a boundary layer are in the order $\delta_{99}$ and these scales are probably also apparent in the spanwise direction; thus the ratio $\delta_{99}/L_z$ should at least be
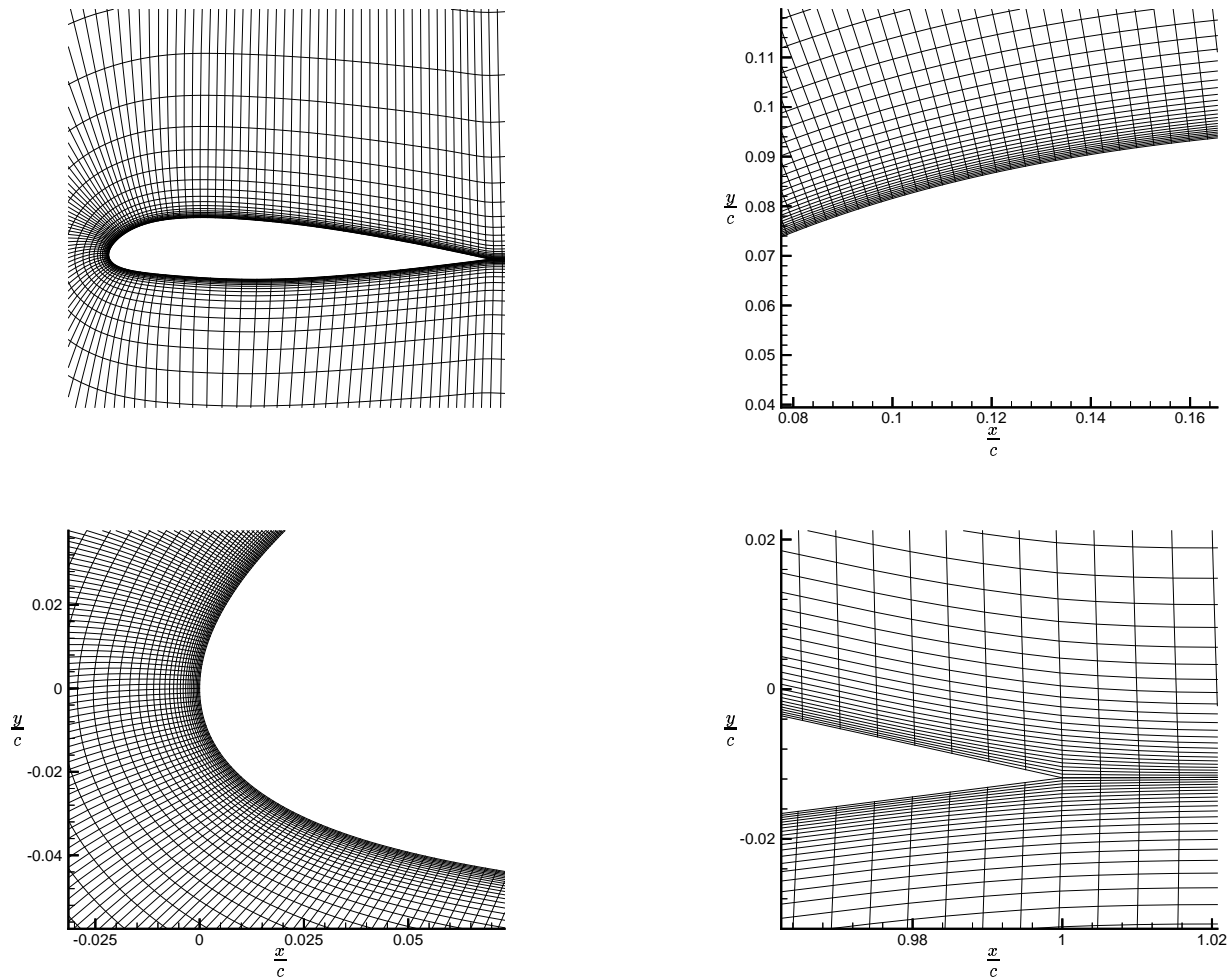
**Fig. 2   Zoom of the mesh at the transition region and at the leading and trailing edges. Every 4th node in the i-direction and every 2nd node in the j-direction are plotted.**

less than one. Near the trailing edge the boundary layer thickness, $\delta_{99}$, from the experiments, is at least 9 % of the chord. Thus, the spanwise extent is believed to be sufficient in this case.

### Parallelization

For the present flow, the required number of nodes in order to do a LES is at least in the order of millions. This is true, even though the transition is prescribed and the effects of the very near-wall structures are modeled by approximate boundary conditions. It is also estimated that about $10 - 20$ time units (1 time unit $= c/U_\infty$, where $c$ is the airfoil chord and $U_\infty$ is the freestream velocity) of simulation are required to be able to gather reliable statistics; with a time step of $3 \cdot 10^{-4} c/U_\infty$ (the present time step), the number of time steps would be at least 33000. The need for an efficient numerical method and effective parallelization is obvious. The present code is parallelized for 3D flows[12] using block decomposition and PVM and MPI as message

passing systems. The code has been ported to a SUN Enterprise 10000 at Chalmers and the IBM SP at the Center for Parallel Computing at KTH.

For the velocities, the convergence criteria is that the $L^1$-norm of the residuals of the discretized momentum equations scaled with $\rho U_\infty A_{inlet} U_\infty$ should be less than the desired convergence level, $\eta$, where $A_{inlet}$ is the projected area of the inlet. Here, the criteria is checked immediately after the solver (but of course without under-relaxation), i.e. the residuals are calculated with the 'old' coefficients and before the correction in the PISO algorithm. For the continuity equation, the criterion is that the $L^1$-norm of discretized finite-volume continuity error scaled with the inlet mass flow should be less than $\eta$.

The computations have been performed on an IBM SP computer at the Center for Parallel Computing at KTH. The computational domain is decomposed into 32 subdomains. The elapsed time per time step is $7s$, with the convergence criteria

fulfilled after two global iterations ($\eta \approx 1 \cdot 10^{-3}$). The simulation of one time unit requires about 180 CPU hours and with MPI and 32 processors the solution is advanced 4 time units per day (24 hours). On this computer, an approximately linear speed-up is obtained between the eight and 32 processor cases.[16,17]

### Boundary Conditions

The inlet is specified all over the curved area of the C-mesh. The velocities are set to $\bar{u} = \cos \alpha U_\infty$ and $\bar{v} = \sin \alpha U_\infty$, where $U_\infty$ is the freestream velocity. At the outlet, a convective boundary condition is applied: $\frac{\partial \phi}{\partial t} + U_\infty \frac{\partial \phi}{\partial x} = 0$. A Neumann boundary condition is used for the pressure at all boundaries ($\frac{\partial \bar{p}}{\partial n} = 0$) and periodic boundary conditions are used in the spanwise direction.

### *Wall Functions*

Numerically, when the near-wall resolution is insufficient, the correct value of the wall shear stress ($\tau_{wall} = \nu \left( \partial \bar{u} / \partial y \right)_{wall}$) needs to be determined. The wall shear stress is usually assumed to be correlated to the velocity in the log region through the use of a near-wall law, e.g. the power law or the log law. In the present work the instantaneous log law is used in the log region ($y^+ \geq 30$):

$$\bar{u}^+ = \frac{\ln y^+}{\kappa} + B \,, \qquad (10)$$

where $\kappa = 0.4$, $B = 5.2$.

The near wall node is often located in the buffer region ($5 \leq y^+ \leq 30$) in which the following wall law is used:

$$\bar{u}^+ = \frac{\ln y^+}{C} + D \qquad (11)$$

Eq. 11 is a matching between the log law (Eq. 10) and the linear law in the viscous sublayer ($y^+ \leq 5$):
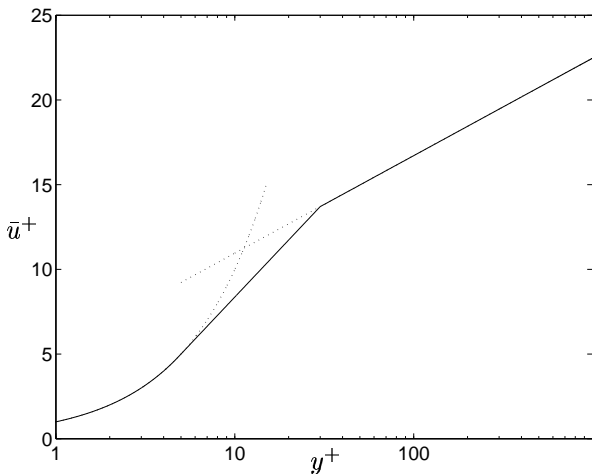
$$\bar{u}^+ = y^+ \qquad (12)$$



**Fig. 3  Plot of the wall functions (Eqs. 10-12).**

The constants in Eq. 11 become $C = \ln 6 / (\frac{1}{\kappa} \ln 30 + B - 5)$ and $D = 5 - \ln 5 / C$.

The approximate wall boundary condition is implemented in the code by adding a viscosity, $\nu_{B.C.}$, to the laminar viscosity on the wall. The friction velocity, $u_\tau$ (and $\tau_{wall}$), is determined from Eqs.10-12. From the relation

$$\frac{\tau_{wall}}{\rho} = u_\tau^2 = \nu \left. \frac{\partial \bar{u}}{\partial y} \right|_{wall} = (\nu + \nu_{B.C.}) \frac{\bar{u}_P}{y_P} \,, \qquad (13)$$

the viscosity on the wall can be expressed as

$$\nu + \nu_{B.C.} = \frac{u_\tau y_P}{\bar{u}_P^+} \qquad (14)$$

Note that the numerical boundary condition for $\bar{u}$, $\bar{v}$ and $\bar{w}$ at the wall is no-slip according to Eq. 13. The product of the artificial viscosity at the wall, $\nu + \nu_{B.C.}$, and the linear velocity assumption between the near-wall node and the wall (see Eq. 13) give the wall shear stress $\tau_{wall}$ according to the wall functions.

## Results

Two computations are presented in this paper. The only set-up difference between the two computations is the SGS model and its treatment in the transition region. The averaging time is nine time units for the simulation with the Smagorinsky model and 5.4 time units for the one-equation SGS model computation. The initial conditions are previous simulations, which originally were started from a 2D $k - \varepsilon$ solution. The time step is $3 \cdot 10^{-4} c / U_\infty$, giving a maximum $CFL$ number of approximately 1.

The transition and growth of the turbulent boundary layer is clearly visualized in the computations, e.g. when looking at instantaneous contour plots of the resolved statistics. The resolved velocity fluctuations in the spanwise direction are shown in the contour plot on the front cover of the paper. The question is if the transition is prescribed in a natural way and if the SGS models are able to model the unresolved stresses in the turbulent boundary layer. Although the computations fail in predicting the trailing edge separation, still some conclusions can be drawn from the results.

Fig. 4 shows the pressure and skin friction coefficient. The pressure peak at the leading edge is overpredicted and we fail to predict the plateau, the decrease in the adverse pressure gradient, that should be present in the separation region. Consequently none of the present computations predict the separation near the trailing edge (a small separation bubble is occasionally instantaneously formed). Note the small plateaus in $C_p$, at about 7 % of the chord for the Yoshizawa SGS model computation and at about 35 % of the chord for the
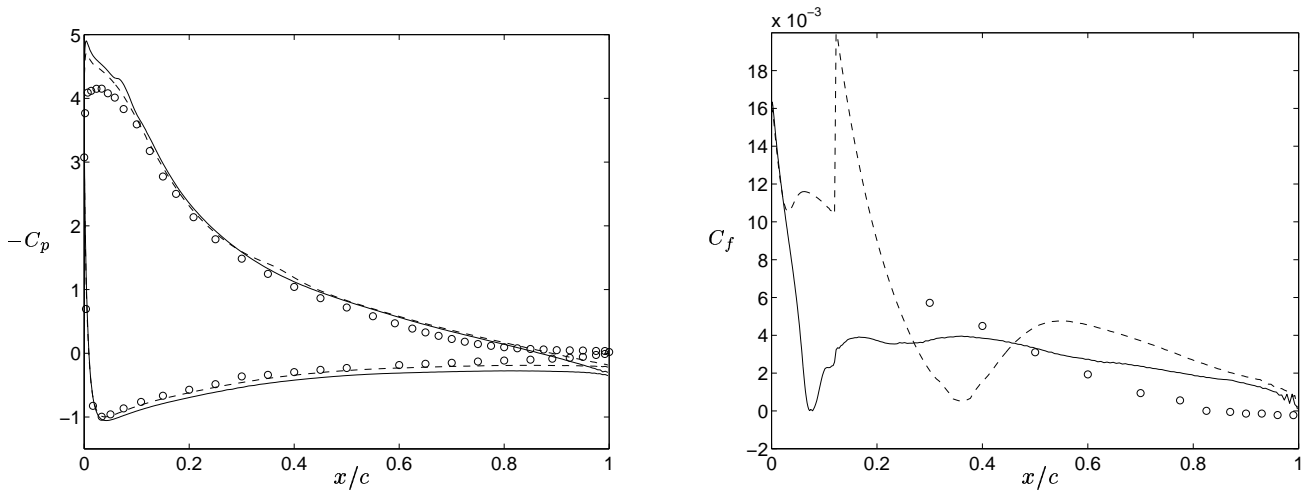
**Fig. 4 The pressure coefficient (left figure) and the skin friction coefficient (right figure). Solid: Yoshizawa one-equation SGS model computation; dashed: Smagorinsky SGS model computation; circles: exp. (F2).**

Smagorinsky computation. They indicate incipient separation bubbles. In the Yoshizawa computation, the predicted incipient separation bubble occurs at approximately the location where the laminar separation bubble was observed in the experiments.

Unfortunately there is no experimental data available in the transition region. Fig. 5(a) shows some statistics at the first node from the wall, at $y_n \approx 0.00013c$, along the suction side of the airfoil. Recall that the Smagorinsky eddy viscosity was blended between 2 % (zero $\nu_{sgs}$) and 12 % of the chord, resulting in a peak in the eddy viscosity at the transition point. Also seen in the near-wall node plot is that there is no wall damping in the Smagorinsky model. The Yoshizawa eddy viscosity was blended between 12 and 23 % of the chord and we get peaks in the resolved stresses at the correct location, at the prescribed transition point. We had hoped that these stresses should trip the boundary layer in a natural way. However, as seen in Fig. 5(a), the stresses are very anisotropic. The Smagorinsky eddy viscosity dampens these unphysical oscillations and we get a transition too far downstream, at about 40 % of the chord. The laminar region is incorrectly captured (see the wall parallel velocity, $\bar{u}_s$, in Fig. 5(a)) and there is a delayed incipient laminar separation at approximately 37 % of the chord (see also $C_f$ in Fig. 4). The laminar region (upstream of the separation region) is better predicted when there is no SGS dissipation in this region (just the dissipation from the upwinding).

Fig. 5(b) shows some statistics away from the wall, at a wall distance of $0.003c$ (the same distance as where the energy spectra in Fig. 7 are collected). The eddy viscosity level is much higher for the Smagorinsky model. However, the reason for the delayed transition in the Smagorinsky com-

putation, is that the Smagorinsky eddy viscosity is *blended* too far upstream. Previous computations have shown that we get a similar transition as for the Yoshizawa computation if the Smagorinsky model is blended downstream of the transition point[16,17] (in Refs. 16 and 17 there are also anisotropic peaks in the stresses at $x/c = 0.12$).

Fig. 6 shows some resolved velocity and stress profiles at four locations on the suction side of the airfoil. The profiles are closer to the experimental results near the trailing edge in the Smagorinsky computation. This is probably fortuitous and owing to the delayed transition.

Wave number energy spectra are shown in Fig. 7 at three locations on the suction side. The very high anisotropy in the stresses is seen in the spectra at 30 % of the chord. Note that for the Smagorinsky computation, this location is upstream of the 'transition point' and consequently the spectra go very steep towards zero at high wave numbers, dampened by the Smagorinsky eddy viscosity. Also, at the other two locations, further downstream, it is seen that the Smagorinsky model is too dissipative at high wave numbers. The Yoshizava eddy viscosity is lower, which is seen in the spectra. The strange behaviour of the longitudinal energy spectra, $E_{ww}$, is probably owing to the far too coarse resolution in the spanwise direction, resulting in unphysical high-frequent oscillations. Looking at the transverse energy spectra, $E_{uu}$ and $E_{vv}$, the resolved scales seem to reach an inertial $-5/3$ range.

The frequency energy spectra in Fig. 7 hardly seem to reach an inertial $-5/3$ range. By using the assumption of 'frozen turbulence',[19] the frequency spectra indicate that the *spatial* streamwise resolution is too coarse. The maximum frequencies that are resolved are in the order of $U_{conv}/2\Delta x$, where $U_{conv}$ is the convective velocity at the point where
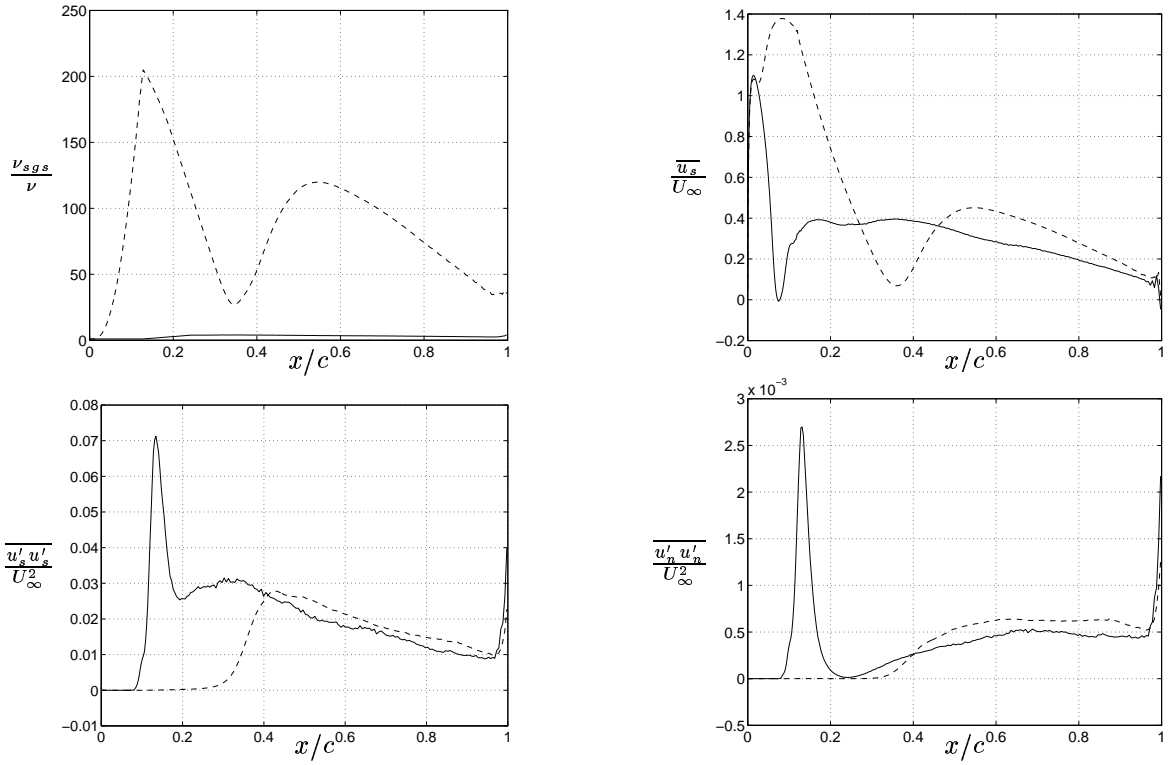
**a)** $y_n = 0.00013c$
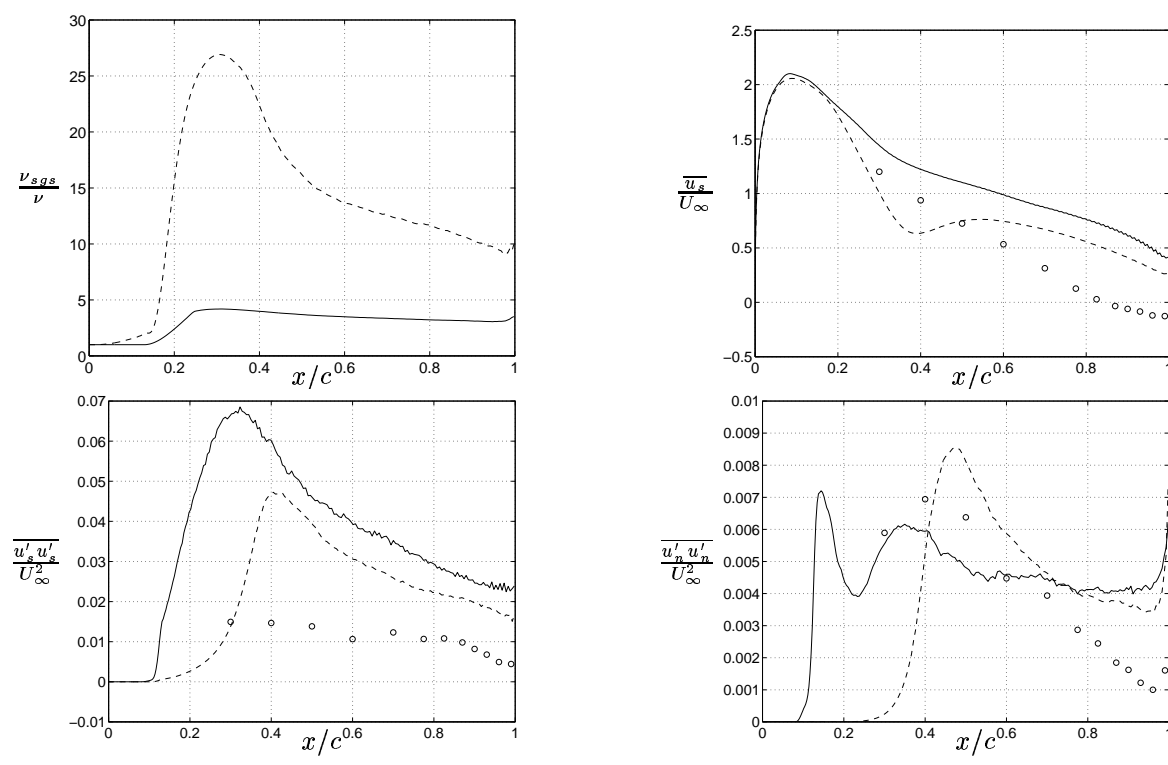


**b)** $y_n = 0.003c$

**Fig. 5   Spanwise and time-averaged first- and second-order statistics along the suction side of the airfoil at $y_n = 0.00013c$ and at $y_n = 0.003c$. Solid: Yoshizawa one-equation SGS model computation; dashed: Smagorinsky SGS model computation; circles: exp. (F2). Subscripts $s$ and $n$ denote the directions parallel and normal to the airfoil wall, respectively.**
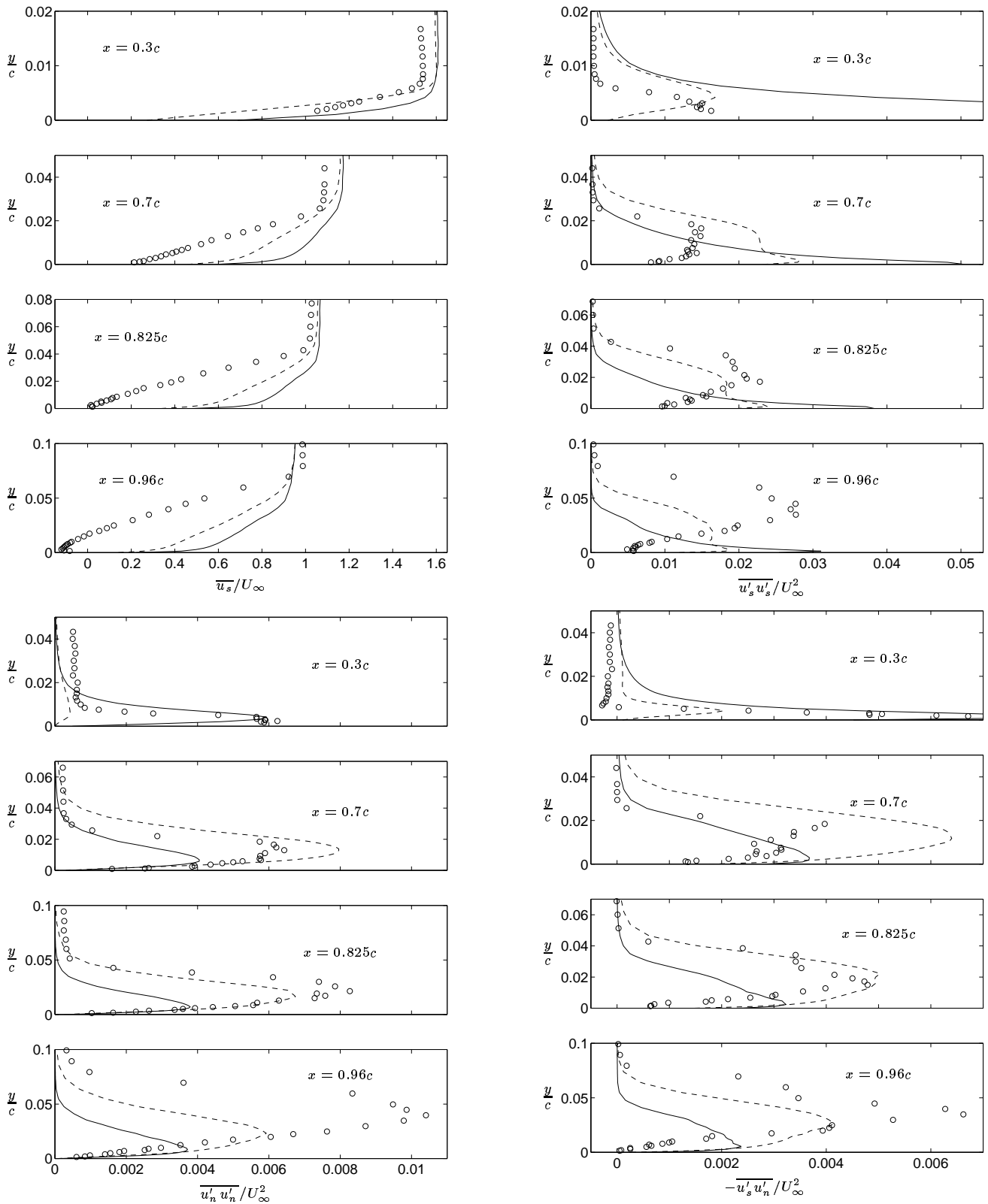
AMERICAN INSTITUTE OF AERONAUTICS AND ASTRONAUTICS, AIAA-2001–0425

**Fig. 6  Spanwise and time-averaged first- and second-order statistics. Solid: Yoshizawa one-equation SGS model computation; dashed: Smagorinsky SGS model computation; circles: exp. (F2). Subscripts $s$ and $n$ denote the directions parallel and normal to the airfoil wall, respectively.**
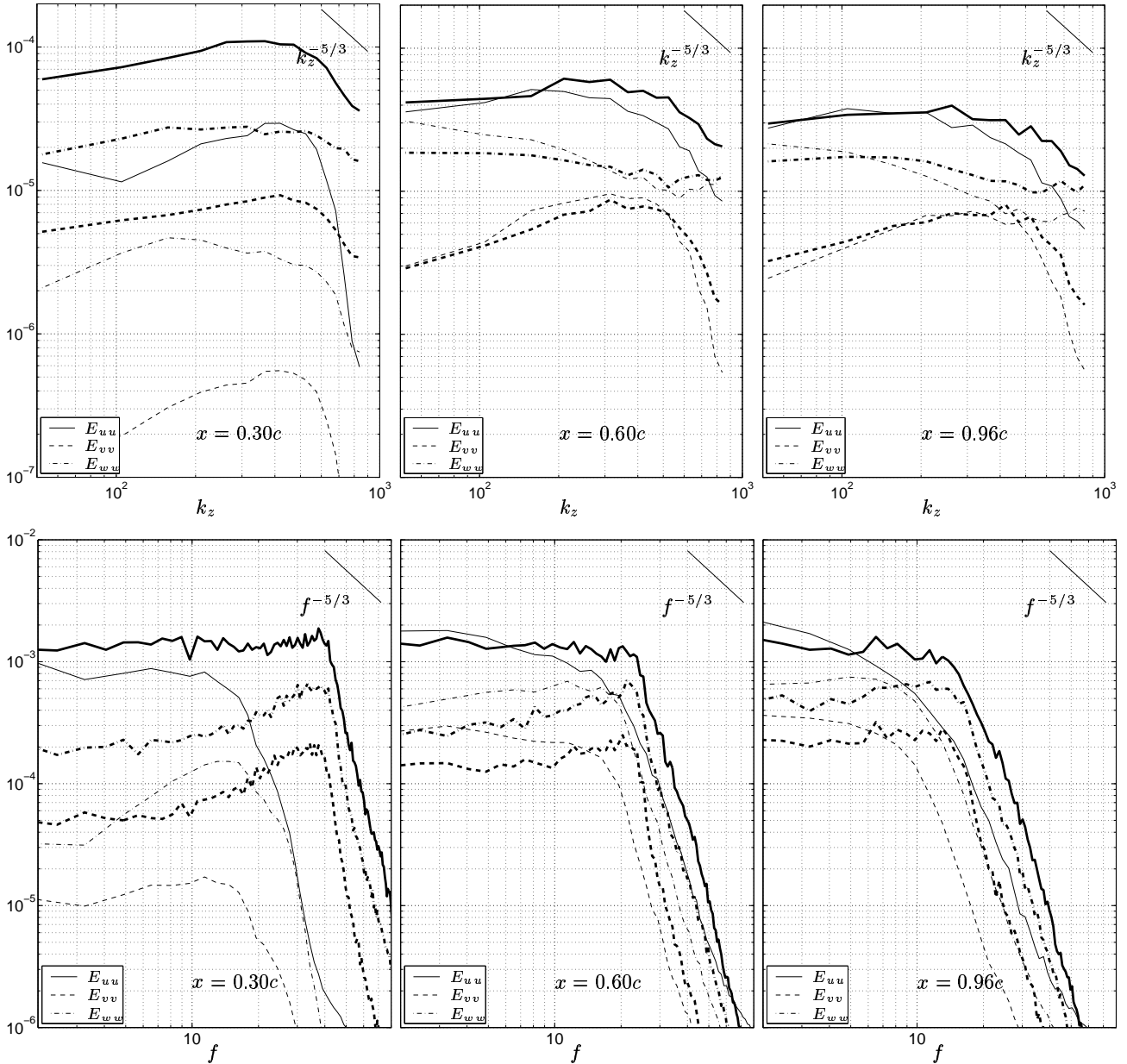
**Fig. 7** Wavenumber and frequency spectra at $y_n = 0.003c$ **(top and bottom figures, respectively). Thick lines: Yoshizawa one-equation SGS model computation; thin lines: Smagorinsky SGS model computation.**

the spectra are collected. This is seen in the frequency spectra as the frequencies where the steep slopes ($f^{-7}$) starts. This occurs, for example, at $f \approx 25$ at $x = 0.6c$. Also, along the suction side wall, the resolution is coarse. Fig. 8 shows the wall resolution in dimensionless wall units based on the predicted friction velocity.

Table 1 shows the lift and drag coefficients for the two computations. The lift coefficients are overpredicted (as expected when there is no trailing edge separation predicted). Figs. 9 and 11 show the time history of the lift coefficients. The signals differ a lot as is also seen in Figs. 10 and 12, which show the frequency spectra of the signals. There is a peak in the frequency spectrum at a Strouhal number

between 8 and 9 in the Smagorinsky computation, whereas it is between 15 and 16 for the Yoshizawa computation. A peak at approximately 8 has also been reported by other partners in the LESFOIL project.[20]

|       | Exp. F1 | Yoshizawa | Smagorinsky |
|-------|---------|-----------|-------------|
| $C_L$ | 1.56    | 1.78      | 1.70        |
| $C_D$ | 0.0204  | 0.0155    | 0.0233      |

**Table 1  Spanwise and time-averaged lift and drag coefficients for the two computations and the experiment in the F1 wind-tunnel.**
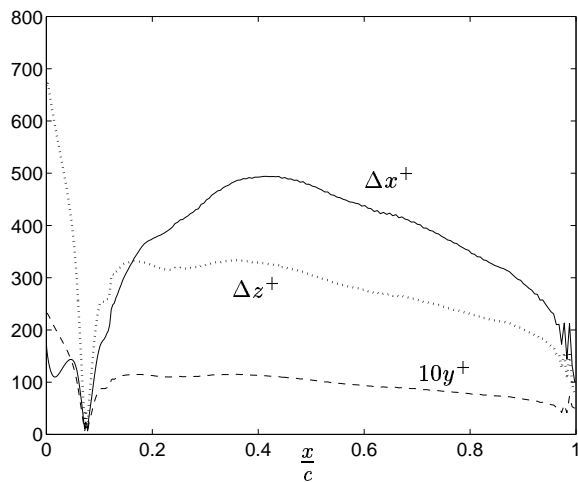
**a)** Yoshizawa one-equation SGS model computation
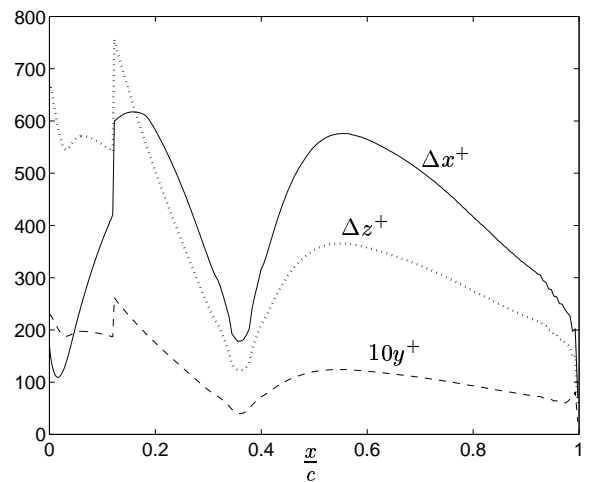


**b)** Smagorinsky SGS model computation

**Fig. 8   Wall resolution along the suction side of the airfoil in dimensionless wall units, based on the predicted friction velocity from the computations.**
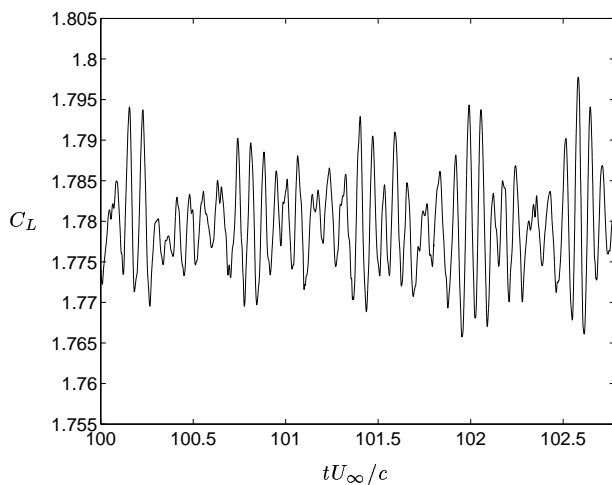


**Fig. 9   Time history of the lift coefficient for the computation with the one-equation SGS model by Yoshizawa.**
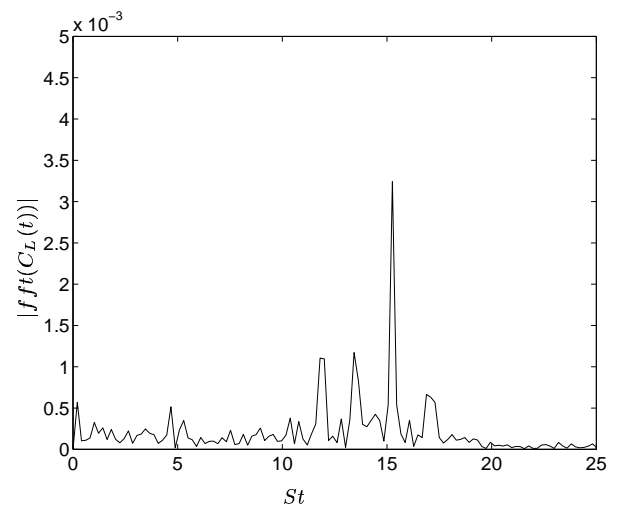


**Fig. 10   Frequency spectrum of the $C_L$ signal for the computation with the one-equation SGS model by Yoshizawa.**
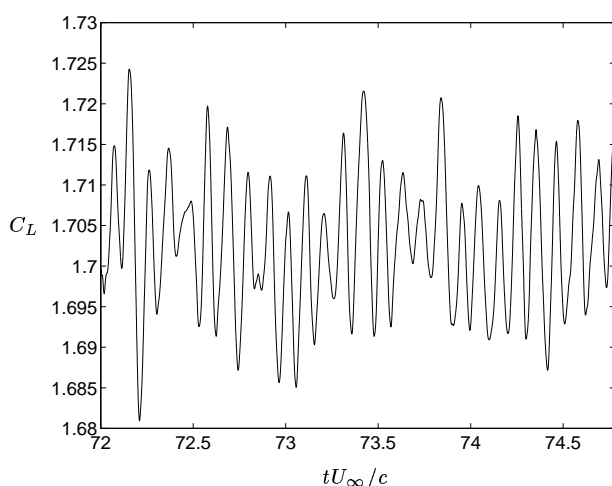


**Fig. 11   Time history of the lift coefficient for the computation with the Smagorinsky model.**
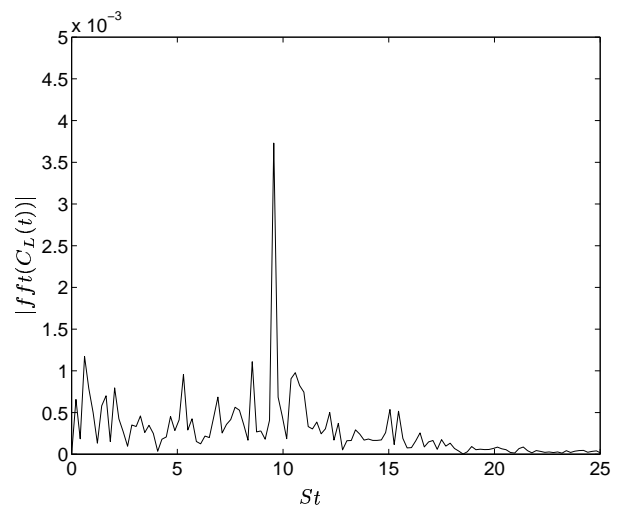


**Fig. 12   Frequency spectrum of the $C_L$ signal for the computation with the Smagorinsky model.**

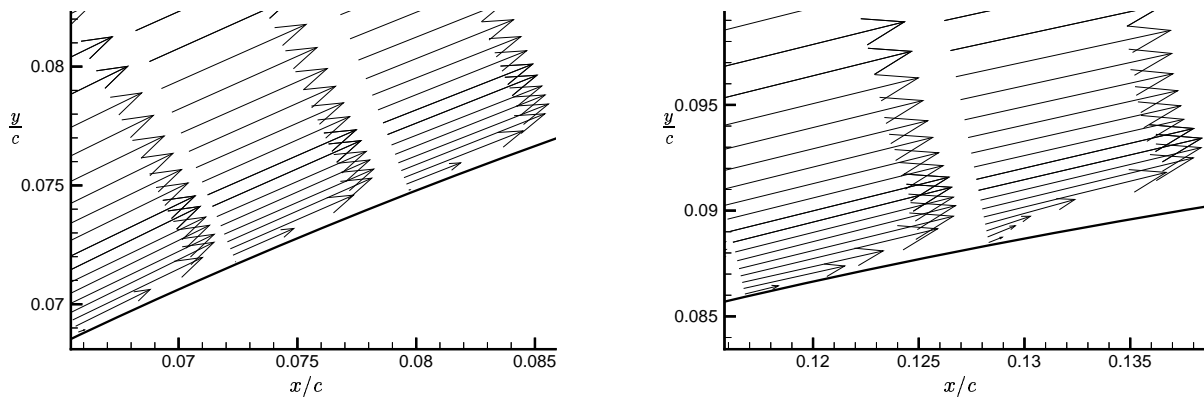AMERICAN INSTITUTE OF AERONAUTICS AND ASTRONAUTICS, AIAA-2001–0425

**Fig. 13 Instantaneous vector plots from the Yoshizawa one-equation SGS model simulation, showing the laminar boundary layer at the incipient separation region (left figure) and the transition region (right figure). Every 4th vector in the streamwise direction is shown.**

## Conclusions and Future Work

With the present treatment of the transition, the transition either takes place too far downstream or, if it occurs at the correct location, it is far too anisotropic and unnatural. However, the laminar region upstream of the transition region is better predicted when there is no SGS dissipation in this region. The transition process and the behaviour of the SGS-models and CDS in that region need further examination to prescribe the transition in a more natural way, using this coarse mesh.

There are deficiencies in the resolution in all of the flow regimes around the airfoil mentioned in the introduction. Because of the strong coupling between the trailing edge separation and the pressure peak at the leading edge, all regions around the airfoil are probably equally important, in order to validate LES (or any other method). Step by step we need to fix the deficiencies and increase the resolution where it is possible. For example, the spanwise extent can probably be narrower and then, with the same number of nodes, the resolution in this direction will increase. In order to impose the transition in a proper way, perhaps a minimum requirement is to resolve the laminar boundary layer and the laminar separation bubble. In the present computations, at the location where the boundary layer is as thickest, there are about 5-6 nodes in the wall-normal direction and the laminar separation bubble is just captured with one node (see Fig. 13). And at the very leading edge ($x/c < 0.01$) there is only one node in the boundary layer.

In future work we are going to increase the resolution in the wall-normal and spanwise direction. The near-wall node will be located at a $y^+ < 1$ and then wall functions do not apply for LES. Future work will instead investigate the use of RANS in the very near-wall region and couple it with LES in the outer region. It might also be easier to pre-scribe the transition with such a hybrid RANS/LES approach.

## Acknowledgements

## References

[1] Davidson, L., "LESFOIL: an European Project on Large Eddy Simulations around a High-Lift Airfoil at High Reynolds Number," *ECCOMAS 2000, European Congress on Computational Methods in Applied Sciences and Engineering, 11-14 September*, Barcelona, Spain, 2000.

[2] "EUROVAL- A European Initiative on Validation of CFD-codes," *Notes on Numerical Fluid Mechanics*, edited by W. Haase, F. Brandsma, E. Elsholz, M. Leschziner, and D. Schwamborn, Vol. 42, Vieweg Verlag, 1993.

[3] "ECARP- European Computational Aerodynamics Research Project: Validation of CFD Codes and Assessment of Turbulence Models," *Notes on Numerical Fluid Mechanics*, edited by W. Haase, E. Chaput, E. Elsholz, M. Leschziner, and U. Müller, Vol. 58, Vieweg Verlag, 1997.

[4] Davidson, L. and Rizzi, A., "Navier-Stokes Stall Predictions Using an Algebraic Stress Model," *J. Spacecraft and Rockets*, Vol. 29, 1992, pp. 794–800.

[5] Davidson, L., "Prediction of the Flow Around an Airfoil Using a Reynolds Stress Transport Model," *ASME: Journal of Fluids Engineering*, Vol. 117, 1995, pp. 50–57.

[6] Lien, F. and Leschziner, M., "Modelling of 2D Separation from High-Lift Aerofoils With a Non-Linear Eddy-Viscosity Model and Second-Moment Closure," *The Aeronautical Journal*, Vol. 99, 1995, pp. 125–144.

[7] Piomelli, U. and Chasnov, J., "Large-Eddy Simulations: Theory and Applications," *Transition and Turbulence Modelling*, edited by D. Henningson, M. Hallbäck, H. Alfredsson, and A. Johansson, Kluwer Academic Publishers, Dordrecht, 1996, pp. 269–336.

[8] Spalart, P., Jou, W.-H., Strelets, M., and Allmaras, S., "Comments on the feasibility of LES for wings, and on a hybrid RANS/LES approach. 1st AFOSR Int. Conf. on DNS/LES, Aug. 4-8, 1997, Ruston, LA," *Advances in DNS/LES, C. Liu & Z. Liu Eds., Greyden Press, Columbus, OH*.

[9] Spalart, P. R., "Private communication," Boeing Commercial Airplanes, 2000.

[10] Davidson, L. and Farhanieh, B., "CALC-BFC: A Finite-Volume Code Employing Collocated Variable Arrangement and Cartesian Velocity Components for Computation of Fluid Flow and Heat Transfer in Complex Three-Dimensional Geometries," Rept. 92/4, Dept. of Thermo and Fluid Dynamics, Chalmers University of Technology, Gothenburg, 1992.

[11] Rhie, C. and Chow, W., "Numerical Study of the Turbulent Flow Past an Airfoil With Trailing Edge Separation," *AIAA Journal*, Vol. 21, 1983, pp. 1525–1532.

[12] Nilsson, H. and Davidson, L., "CALC-PVM: A Parallel Multiblock SIMPLE Multiblock Solver for Turbulent Flow in Complex Domains," Tech. Rep. 98/12, Dept. of Thermo and Fluid Dynamics, Chalmers University of Technology, Gothenburg, 1998.

[13] Issa, R., "Solution of Implicitly Discretised Fluid Flow Equations by Operator-Splitting," *J. Comp. Physics*, Vol. 62, 1986, pp. 40–65.

[14] Smagorinsky, J., "General Circulation Experiments With the Primitive Equations," *Monthly Weather Review*, Vol. 91, 1963, pp. 99–165.

[15] Yoshizawa, A., "Statistical Theory for Compressible Shear Flows with the Application of Subgrid Modelling," *Physics of Fluids A*, Vol. 29, 1986, pp. 2152–2163.

[16] Dahlström, S. and Davidson, L., "Large Eddy Simulation of the Flow around an Aerospatiale A-Aerofoil," *ECCOMAS 2000, European Congress on Computational Methods in Applied Sciences and Engineering, 11-14 September*, Barcelona, Spain, 2000.

[17] Dahlström, S., "Large Eddy Simulation of the Flow around a High-Lift Airfoil," Thesis for the degree of Licentiate of Engineering 00/5, Dept. of Thermo and Fluid Dynamics, Chalmers University of Technology, Gothenburg, Sweden, 2000.

[18] Gough, T., Gao, S., Hancock, P., and Voke, P. R., "Experiment and simulation of the tripped boundary layer on a flat plate: Comparative study," Tech. Rep. ME-FD/95.40, Dept. of Mechanical Engineering, The University of Surrey, U.K., 1996.

[19] Frost, W., "Spectral Theory of Turbulence," *Handbook of Turbulence*, edited by W. Frost and T. Moulden, Vol. 1, Plenum Press, New York, 1977, pp. 85–125.

[20] "30-months report, LESFOIL: A Brite-Euram project," Tech. rep., 2000.